Low Temperature Physics/Fizika Nizkikh Temperatur, 2015, v. 41, No. 12, pp. 1237–1242

Complex conductance of ultrathin $La_{2-x}Sr_xCuO_4$ films and heterostructures

V.A. Gasparov

Institute of Solid State Physics RAS, Chernogolovka, Moscow district 142432, Russia
E-mail: vgasparo7@gmail.com

I. Božović

Brookhaven National Laboratory, Upton, NY 11973, USA

Applied Physics Department, Yale University, New Haven CT 06520, USA

Received June 11, 2015, published online October 23, 2015

We used atomic-layer molecular beam epitaxy to synthesize bilayers of a cuprate metal ($La_{1.55}Sr_{0.45}CuO_4$) and a cuprate insulator (La_2CuO_4), in which each layer is just one unit cells thick. We have studied the magnetic field and temperature dependence of the complex sheet conductance, $\sigma(\omega)$, of these films. Experiments have been carried out at frequencies between 2–50 MHz using the single-spiral coil technique. We found that: (i) the inductive response starts at $\Delta T = 3$ K lower temperatures than Re $\sigma(T)$, which in turn is characterized by a peak close to the transition, (ii) this shift is almost constant with magnetic field up to 14 mT; (iii) ΔT increases sharply up to 4 K at larger fields and becomes constant up to 8 T; (iv) the vortex diffusion constant $D(T)$ is not linear with T at low temperatures as in the case of free vortices, but is rather exponential due to pinning of vortex cores, and (v) the dynamic Berezinski–Kosterlitz–Thouless (BKT) transition temperature occurs at the point where $Y = (l_\omega/\xi_+)^2 = 1$. Our experimental results can be described well by the extended dynamic theory of the BKT transition and dynamics of bound vortex–antivortex pairs with short separation lengths.

PACS: 74.78.Fk Multilayers, superlattices, heterostructures;
74.72.Gh Hole-doped;
74.40.−n Fluctuation phenomena.

Keywords: superconducting heterostructures, high-frequency conductivity, Berezinski–Kosterlitz–Thouless transition.

Ultrathin films of high-temperature superconductors have been studied intensely, with numerous attempts to observe the Berezinski–Kosterlitz–Thouless (BKT) transition [1–19]. For example, a few unit-cell (UC) thick $YBa_2Cu_3O_{7-x}$ (YBCO) films sandwiched between semiconducting or insulating layers have broader resistive transitions than thicker ones, which have been attributed to the BKT physics [4–6]. The same explanation was proposed for the observation of nonlinear current-versus-voltage (I–V) characteristics in YBCO, BiSrCaCuO, and TlBaCaCuO single crystals and thin films (see Ref. 7 and references therein). This has been a matter of substantial debate, though. For example, Repaci *et al.* [8] found the I–V characteristics to be ohmic even in 1 UC thick YBCO films at temperatures below the critical temperature (T_c), indicating the absence of the BKT transition. Subsequently, however, it was shown that at low currents the addition of current noise can turn nonlinear I–V curves into ohmic behavior [9]. Thus, it is easy to confuse nonlinear I–V tails generated by noise with non-ohmic tails expected from the BKT transition. Moreover, it was recently shown that the size effects may radically alter the I–V curves of superconducting films [10] so that they mimic the dc BKT behavior. Thus, it is important to understand that nonlinear I–V characterizes *per se* cannot prove the occurrence of the BKT transition; one needs to see a concurrent sharp drop in the superfluid density.

Further, it was noted that a precondition [8] for the BKT transition to occur in a superconductor, i.e., that the sample size $L_s < \lambda_{\text{eff}}$, where $\lambda_{\text{eff}} = 2\lambda^2/d$ is the effective (Pearl) penetration depth and d is the film thickness, is not satisfied even in 1 UC thick YBCO films [11]. Next, Davis

et al. [13] made a detailed comparison of the experimental data taken from YBCO films [12] with the BKT theory and found disagreement, which was attributed to inhomogeneity and vortex pinning. Finally, Rogers *et al.* [14] measured low-frequency noise in ultrathin $Bi_2Sr_2CaCu_2O_8$ films and reported absence of thermally activated vortices and BKT transition, again attributing this to vortex pinning. Hence, it is still controversial not only whether the true BKT transition has been observed in cuprates so far, but even whether it can occur at all in superconducting films.

On the other side, Minnhagen [15] suggested that although the usual BKT transition is not present when $L_s > \lambda_{\text{eff}}$, it is still possible to observe at high frequencies the BKT-like response from the bound pairs such that the vortex separation length $r < \lambda_{\text{eff}}$. According to the BKT theory extended to finite frequencies [15–17], higher-frequency currents largely probe vortex–antivortex pairs of smaller separations. At high frequency, the electromagnetic response of a 2D superconductor is dominated by those bound pairs that have $r \sim l_\omega$, where $l_\omega = (14D/\omega)^{1/2}$ is the vortex diffusion length and D is the vortex diffusion constant. Using the Bardeen–Stephen formula for free vortices, $D = 2e^2\xi_{GL}^2 k_B T/(\pi\hbar^2\sigma_n d)$ [18], at $\omega \geq 10$ MHz we estimate that $l_\omega < 1$ μm, which is much less than $\lambda_{\text{eff}} \sim 40$ μm as found in 1 UC thick YBCO films. This implies that it should be possible to detect the response of vortex–antivortex pairs with short separation lengths at radio (rf) and microwave (μW) frequencies in ultrathin cuprate films, even though the usual BKT transition is not seen in dc and low-frequency measurements.

Recently, we reported the frequency and temperature dependences of the complex sheet conductance, $\sigma(\omega,T)$, of 1 to 3 UC thick YBCO films sandwiched between semiconducting $Pr_{0.6}Y_{0.4}Ba_2Cu_3O_{7-x}$ layers [7,19], and in bilayers of a cuprate metal, $La_{1.55}Sr_{0.45}CuO_4$ (LSCO) and a cuprate insulator, La_2CuO_4 (LCO), in the frequency range 0.023 MHz $< \omega <$ 50 MHz [20,21]. In these samples, as the frequency is increased, we observed a significant increase of T_c. A maximum in Re $\sigma(T)$ near T_c and a jump in superfluid density were observed as well, and moreover the scaling of the jump with the frequency and temperature was found to be very close to the theoretical prediction. The superfluid jump was suppressed in a small magnetic field, the magnitude of which increased with the frequency. Vortex pinning with thermally activated vortex diffusion constant was observed in these samples, but it did not destroy the vortex–antivortex pairs with short separation lengths. The results reviewed below indicate that such bilayers are a very good 2D model system for studying the physics of the dynamic BKT transition.

Experimental

We have grown bilayer LSCO/LCO films in a unique atomic-layer-by-layer molecular beam epitaxy (ALL-MBE) system [22] that incorporates *in situ* surface science tools such as time-of-flight ion scattering and recoil spectroscopy (TOF-ISARS) and reflection high-energy electron diffraction (RHEED). ALL-MBE enables synthesis of atomically smooth films as well as of multilayers with perfect interfaces [23,24]. Typical surface roughness determined from atomic force microscopy (AFM) data is 0.2–0.5 nm, less than 1 UC height which in LSCO is 1.3 nm. The films were grown on single-crystal $LaSrAlO_4$ substrates polished perpendicular to the [001] crystal direction, so that the c axis of LSCO was normal to the film surface. The microstructure, growth mechanism of LSCO/LCO films, and their superconducting properties have been reported before [23,24].

We have used a contactless, single-coil inductance technique [25,26] to measure the absolute value of magnetic field penetration depth, $\lambda(T)$, in superconducting thin film samples. This technique, originally proposed by Gasparov and Oganesyan [25] and improved in [26], has the same advantages as the two-coil technique [27–30], while it has much higher sensitivity to the variations of $\lambda(T)$, etc. [26]. This technique was extensively used for the study of the $\lambda(T)$ dependence for YBCO, ZrB_{12}, and MgB_2 single crystals and thin films [31,32].

In this rf technique, we measure the change of mutual inductance, ΔM, between a film and a one-layer pancake coil with diameter 1 mm. This coil is located in the proximity of the film and connected in parallel to a capacitor C. The LC circuit is driven by a TE 1000 RF Vector Impedance Analyzer operating at 0.5–150 MHz, with a high frequency stability of 1 Hz. An impedance meter (VM-508 TESLA) operating at 2–30 MHz, with a high frequency stability of 10 Hz, was used as well. The film is placed in vacuum, at a small distance (~ 0.1 mm) above the coil; this allows the sample temperature to vary from room temperature down to 1.2 K. The instrument measures the impedance as a function of frequency, which is scanned near the resonant one. Thus we determine the resonance frequency and the impedance (at resonance) as a function of the temperature. Since in our bilayer films the superconducting layer thickness d = 0.2–0.5 nm $<< \lambda$, the change in the complex mutual inductance of the coil, $M(T)$, that occurs because of the superconducting transition in the film, may be written as [26]

$$\text{Re}\, M(T) = L_0\left[1-\left(\frac{f_0}{f(T)}\right)^2\right] = -i\pi\mu_0\int_0^\infty \frac{M(x)\,dx}{1+2x\lambda\,\coth(d/\lambda)}. \quad (1)$$

Here

$$M(x) = \left[e^{-hx}\sum_{m=0}^{N-1}(r+m\Delta R)J_1\left[x(r+m\Delta r)\right]\right]^2 \quad (2)$$

is the self-inductance of the coil without the sample, x is the wave number in the xy plane, h is the sample-coil distance, r is the internal radius of the one-layer spiral coil, Δr is the spacing between adjacent turns of the coil, d is the

film thickness, and μ_0 is the free-space permeability. The range of values of x giving the dominant contribution to $M(x)$ is very small, on the order of the inverse of the internal diameter of the coil (~0.25 mm). In the London regime, mainly the inductive part of the coil impedance is changed during the superconducting transition. This change is detected as a change of the frequency $f(T)$ and converted into the variation of $\lambda(T)$ using Eqs. (1) and (2), where

$$l = \sqrt{\left[i\omega\mu_0(\sigma_1 - i/(\omega\mu_0\lambda^2)\right]^{-1}} \qquad (3)$$

is a complex length. Here σ_1 is the real part of the film conductivity, $\sigma(\omega,T) = \sigma_1(\omega,T) - i\,[\omega L_k(\omega,T)]^{-1}$, where $\sigma_1(\omega,T)$ is the dissipative component of the sheet conductance and $L_k(\omega,T) = \mu_0\lambda^2/d$ is the sheet kinetic inductance. By replacing $\sigma_1 = 0$ and keeping in mind that $d << \lambda$, we obtain the final expression for the variation of the mutual inductance between the coil and the film:

$$\mathrm{Re}\,M \approx -\frac{\pi\mu_0}{\lambda^2}\int_0^\infty \frac{dM(x)}{2x}dx, \qquad (4)$$

$$\mathrm{Im}\,M \approx \pi\mu_0{}^2\omega\sigma_1\int_0^\infty \frac{dM(x)}{2x}dx. \qquad (5)$$

The change of the imaginary part of M with temperature can be determined [26] from the real part of the LC circuit impedance Re $Z(T)$, by means of the equation

$$\mathrm{Im}\,M(T) = \frac{1}{2\pi f^3(T)C^2}\left[\frac{1}{\mathrm{Re}\,Z(T)} - \left(\frac{f(T)}{f_0}\right)^2\frac{1}{\mathrm{Re}\,Z_0}\right]. \qquad (6)$$

Here f_0 and Re Z_0 are the resonant frequency and the impedance of the LC circuit above T_c.

We have also used two-coil mutual inductance technique. In these experiments, the film is clamped between two axially symmetric coils of the average radius 1 mm. The in-phase and quadrature components of the voltage at the receiving coil, in response to an ac current in the drive coil, are detected by conventional lock-in techniques [27–30]. For our films with $d << \lambda$ the in-phase signal is roughly proportional to the mutual inductance between the drive and pick-up coils: $M(T) \approx M_0(2\lambda^2/Rd)$, while the quadrature signal is proportional to the imaginary part of $M(T)$, where M_0 is the mutual inductance between the coils without the film, d is the film thickness, and R is the effective radius of the coils.

We used a two-stage Gifford–McMahon cryocooler from ULVAC technologies Inc., with a UR4K03 cold head combined with a C10 compressor, running on 60 Hz power. We customized it by adding a thermal damping system that we have developed, providing temperature stabilization to sub-mK level in the entire region of 3 K < T < 300 K [33]. For temperature control, a heater driven by a commercial temperature controller (Lake Shore 340) is mounted on the sample stage. The sample with sapphire holder was mounted either horizontally or vertically. A copper solenoid coil placed on the top of the cryocooler head allowed us to apply a small magnetic field (~100 G) either perpendicular or parallel to the film surface. Additional measurements have been done in a superconducting magnet with fields up to 9 T.

Results

The inversion from $M(T)$ in single-coil technique to $\lambda(T)$ and $\sigma(T)$ is simple compared to the more familiar two-coil mutual inductance technique [27–30]. Calculating the integrals in Eqs. (4) and (5), one gets the values of Re $M(T)$ and Im $M(T)$ at a fixed temperature. Thus we get $\lambda(T)$ and finally the kinetic inductance of the film, $L_k^{-1}(T) = \mu_0\lambda^2/d$, and the high-frequency conductivity, $\sigma(\omega,T)$, shown in Figs. 1 and 2.

We found that $L_k^{-1}(T)$ fits well over a wide temperature range to a parabolic dependence [34]: $L_k^{-1}(T) = L_k^{-1}(0)\times$ $\times[1-(T/T_{co})^2]$, shown as thin solid lines in Fig. 1. The mean-field transition temperature, T_{co}, determined by extrapolation of the parabolic dependence of $L_k^{-1}(T)$ to 0, is larger than the onset point of the experimental $L_k^{-1}(T)$ transitions by 4 K, while it is the same as the onset point of $\omega\mathrm{Re}\,\sigma(T)$. We emphasize that this quadratic equation fits the data below a characteristic temperature that we denote as T_{BKT}^{dc}, which is lower than T_{BKT}^{ω}, the position of the peak in ω Re $\sigma(T)$.

In Fig. 3 we show the values of $L_k^{-1}(T)$ and ω Re $\sigma(T)$ of a metal–insulator (M–I) bilayer film with a higher T_c, measured at different frequencies, 8 MHz < ω < 51 MHz, in single-coil inductance experiments. One can notice

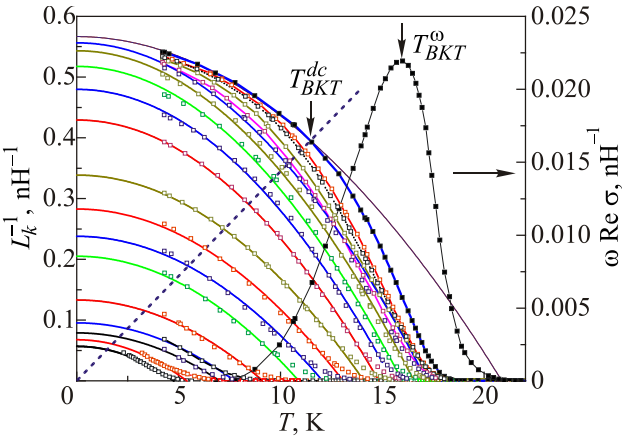

Fig. 1. (Color online) Temperature dependences of $L_k^{-1}(T)$ and ω Re $\sigma(T)$ for bilayer film at 8 MHz and different magnetic fields perpendicular to the film surface: B = 0; 0.0014; 0.0023; 0.003; 0.006; 0.013; 0.019; 0.036; 0.1; 0.2; 0.4; 0.6; 1.0; 1.5; 2.0; 3.4; 4.6; 5.2; 6.0; 7.0 T. The solid lines are quadratic fits to $L_k^{-1}(T)$ below T_{BKT} at different magnetic fields. Also shown is the theoretical BKT function (dashed line).

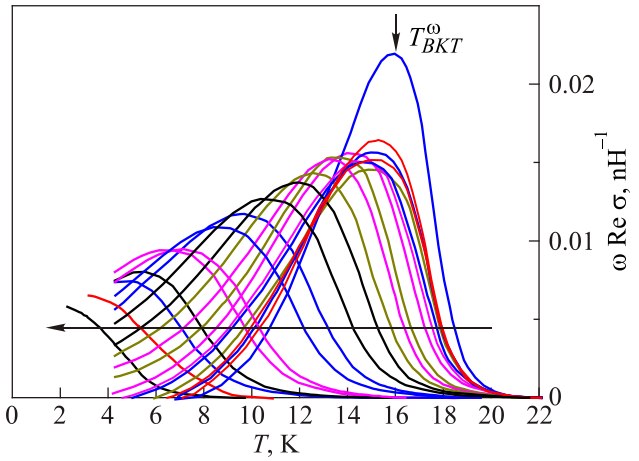

Fig. 2. (Color online) Temperature dependences of ω Re σ(T) at the same magnetic fields as in Fig. 1.

a large frequency dependence of T_c — the temperature at which the superconducting transition onsets becomes apparent, is continuously increases with ω up to 51 MHz, in both $L_k^{-1}(T)$ and ω Re σ(T). Apart from this, we also observed a small difference, $\Delta T = 0.22$ K, in the onsets Re $M(T)$ and Im $M(T)$, for low-frequency data as well, from two-coil mutual inductance data taken at 23 kHz.

Analysis and discussion

In order to see whether this assumption about the BKT transition is correct, in Fig. 1 we plot the theoretical BKT function $L_k^{-1}(T)$ (the dashed straight line) derived from the universal relationship:

$$L_k^{-1}\left(T^{dc}_{BKT}\right) = \frac{32\pi^2 k_B T^{dc}_{BKT}}{\phi_0^2 \mu_0} = T^{dc}_{BKT}/12.3 \ \text{[nH·K]} \quad (7)$$

predicted by the BKT theory [11].

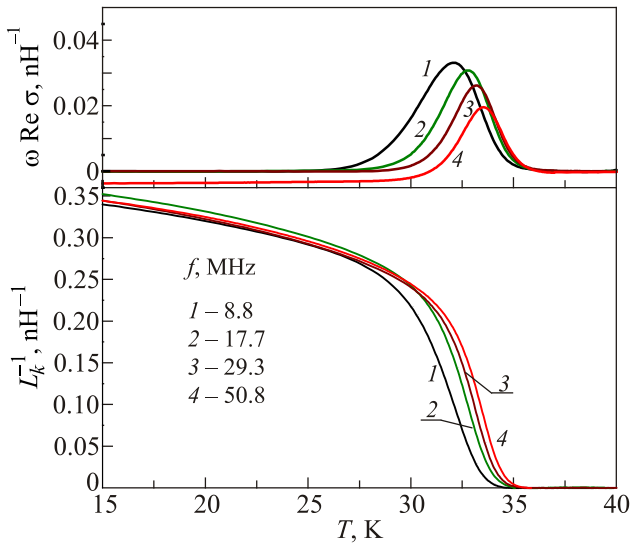

Fig. 3. (Color online) Temperature dependences of $L_k^{-1}(T)$ and ωRe σ(T) for a LSCO/LCO bilayer film with a higher T_c, measured by the single-coil inductance technique at 8.8–50.8 MHz.

Notice however, that this theoretical dependence (Eq. (7)) is valid for the dc case. The observed high-frequency response is dominated by the pairs with the vortex separation length $r \sim l_\omega \sim \omega^{-1/2}$ and therefore T^{ω}_{BKT} must increase with the frequency. This is why the critical temperature determined from the intercept of the dashed theoretical line with the experimental $L_k^{-1}(T)$ curve is lower then T^{ω}_{BKT}. Note also that there is some uncertainty about the exact thickness of the superconducting fluid in the LSCO/LCO bilayer films [24].

Another test for T^{ω}_{BKT} can be made by analyzing the onset points of strong dependences of $L_k^{-1}(T)$ and ω Re σ(T) on the frequency. A central quantity in the dynamic description of BKT transition is the frequency-dependent complex dielectric function ε(ω) which describes the response of a 2D superconductor to an external time-dependent field. The measured $L_k^{-1}(T)$ is renormalized from the value $L_{k0}^{-1}(T)$ in the absence of vortices: $L_{k0}^{-1}(T)/L_k(T) = n_s/n_{0s} = \text{Re}\,[1/\varepsilon(\omega)]$.

After Refs. 3 and 11, one can derive the following relation in the high-frequency limit:

$$\frac{L_k^{-1}(T)}{\omega \,\text{Re}\,\sigma} = \frac{\pi(Y-1)}{2Y \ln Y}, \quad (8)$$

where $Y = (l_\omega/\xi^+)^2$, $l_\omega = 14D/\omega^{1/2}$ is the vortex diffusion length and D is the vortex diffusion constant. Both real and imaginary part of the $1/\varepsilon(\omega)$ are directly related to $Y(T)$ [3]. Using the $L_k^{-1}(T)$ and ω Re σ(T) data from Figs. 1 and 2, we solved Eq. (1) for $Y(T)$ and in Fig. 4 plotted Y versus $(1/T - 1/T_{BKT})$ curves. Here T^{ω}_{BKT} is a temperature where $Y = 1$.

The qualitative explanation of the $Y(T)$ dependence shown in Fig. 4 is as follows. By probing the system at

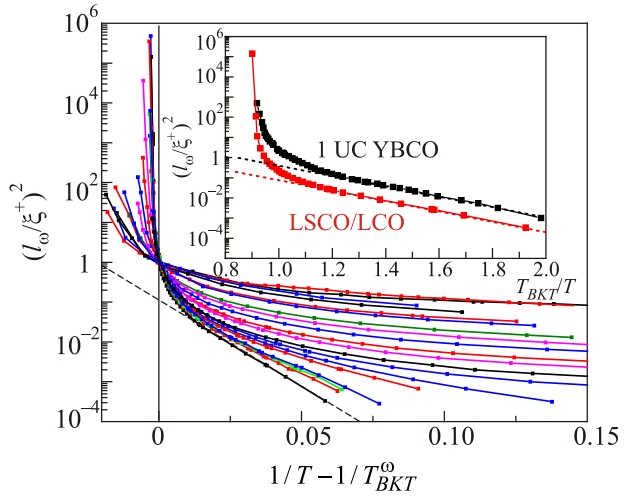

Fig. 4. (Color online) Temperature dependences of $Y = (l_\omega/\xi^+)^2$ at different magnetic fields perpendicular to the film face, B = 0; 0.0014; 0.0023; 0.003; 0.006; 0.013; 0.019; 0.036; 0.1; 0.2; 0.4; 0.6; 1.0; 1.5; 2.0; 3.4; 4.6; 5.2; 6.0; 7.0 T. Inset shows the Y versus T_{BKT}/T dependences for LSCO/LCO heterostructure and 1 unit cell thick YBCO film [7].

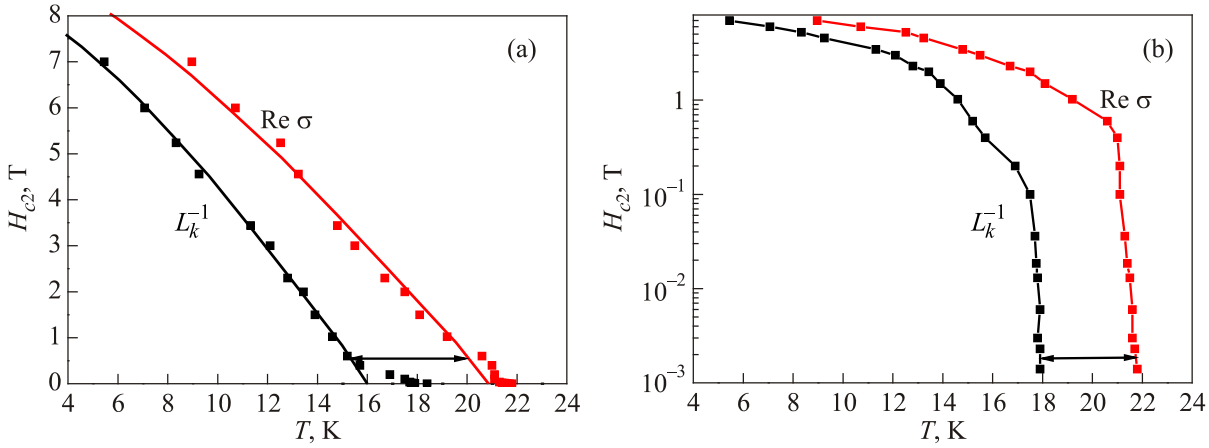

Fig. 5. (Color online) (a) $H_{c2}(T)$ determined as the onsets of $L_k^{-1}(T)$ and Re σ(T) field dependences. The solid lines indicate the temperature dependences according to the WHH model. (b) $H_{c2}(T)$ curves present the same data on the log scale. The solid lines are guide to the eye.

finite frequencies, the observed bound-pair response is dominated by those pairs with $r \sim l_\omega$. At temperatures below T_{BKT}^{dc}, the dissipation is proportional to the number of such vortex–antivortex pairs [11,15]. This number grows gradually with temperature up to T_{BKT}^{ω}. On the high-temperature side, Re σ decreases with increasing temperature since $\mathrm{Re}\,\sigma \propto 1/n_f\mu$, where n_f is the density of free vortices and μ is the vortex mobility [11]. Dissipation is the largest when the correlation length $\xi^+(T)$, i.e., the average distance between thermally induced free vortices above T_{BKT}^{ω}, becomes equal to l_ω, which determines the BKT transition temperature at a given frequency, T_{BKT}^{ω}. This transition temperature is determined as the point at which $Y = 1$ (corresponding to the maximum of ω Re σ(T) curve) and is frequency-dependent due to $r \sim l_\omega$ relation.

From the $Y(T)$ data on the low-temperature side (Fig. 4), we found that the vortex diffusion constant $D(T)$ is not linear with T at low-temperature range as is the case for free vortices [11]. Rather, the data can be fitted with an exponential dependence $D(T) = D_0 \exp\left[E_0/k_B(1/T - 1/T_{BKT}^{\omega})\right]$, which can be attributed to pinning of vortex cores [11]. The pinning energy, $E_0/k_B = 52$ K, decreases with H down to 16 K for $H = 0.2$ T and then is almost H-independent for $H > 0.2$ T. On the high-temperature side, the $Y(T)$ curves deviate from the exponential form due to temperature dependence of $\xi^+(T)$ but they collapse onto a single curve for $H < 0.2$ T, indicating that the temperature dependence of $\xi^+(T)$ is the same for these fields. The Abrikosov vortex lattice parameter $a_v = (\phi_0/H_{\mathrm{ext}})^{1/2}$ ($1.02\cdot10^{-5}$ cm at 0.2 T) is the scale limiting the formation of vortex–antivortex pairs in a magnetic field [13]. We can estimate the field H_{ext} which destroys the vortex pair unbinding from the following relation: $l_\omega \sim a_v$. Apparently, this is the reason why the $Y(T)$ curves deviate from the single one for $H > 0.2$ T, due to the destruction of the dynamic BKT transition by the magnetic field.

Another test for T_{BKT}^{ω} can be made by analyzing the onset points of strong dependences of $L_k^{-1}(T)$ and ω Re σ(T) on the magnetic field perpendicular to the film surface, which we denote as $H_{c2}(T)$. As one can see from Fig. 5, the onset point for $L_k^{-1}(T)$ is shifted downwards with respect to the onset of ω Re σ(T) by a nearly constant value of about 4 K. This $H_{c2}(T)$ dependence is rather peculiar. It follows that there are three "critical" temperatures, (i) the mean-field value $T_{c0} = 20.9$ K, (ii) $T_{BKT}^{\omega} = 19$ K, and (iii) $T_{BKT}^{H} = 16$ K due to the destruction of the BKT transition by the magnetic field. This is clear from the log H_{c2} vs T plot shown on the right-hand side in Fig. 5. We can see the break in the slope of $H_{c2}(T)$ inferred from $L_k^{-1}(T)$ which is absent in $H_{c2}(T)$ determined from ω Re σ(T).

Figures 6(a) and (b) show similar two-step behavior of $H_{c2}(T)$ observed in one-unit-cell-thick $YBa_2Cu_3O_{7-x}$ films sandwiched between semiconducting $Pr_{0.6}Y_{0.4}Ba_2Cu_3O_{7-x}$ layers [7]. Here we plot the $H_{c2}(T)$ data from Re $M(T)$ and Im $M(T)$ curves, showing almost the same difference in T_c (3 K).

Conclusions

In conclusion, we have studied the dependences of the real and the imaginary parts of complex sheet conductance, σ(ω), on the magnetic field and temperature, in LSCO/LCO bilayer films as well as in one-unit-cell-thick YBCO films sandwiched between semiconducting $Pr_{0.6}Y_{0.4}Ba_2Cu_3O_{7-x}$ layers. Our rf measurements on these films showed three key features: (i) a steep jump in $L_k^{-1}(T)$, (ii) a maximum in ω Re σ(T), and (iii) a systematic downward shift of the T_c onset point of $L_k^{-1}(T)$ curves compared to the transition onset of ω Re σ(T) curves. Magnetic field $H > 0.2$ T removes the steep jump of $L_k^{-1}(T)$ but it does not change the temperature shift. Although the first two features are in agreement with the dynamic BKT model, independence of the shift on the magnetic field is rather surprising.

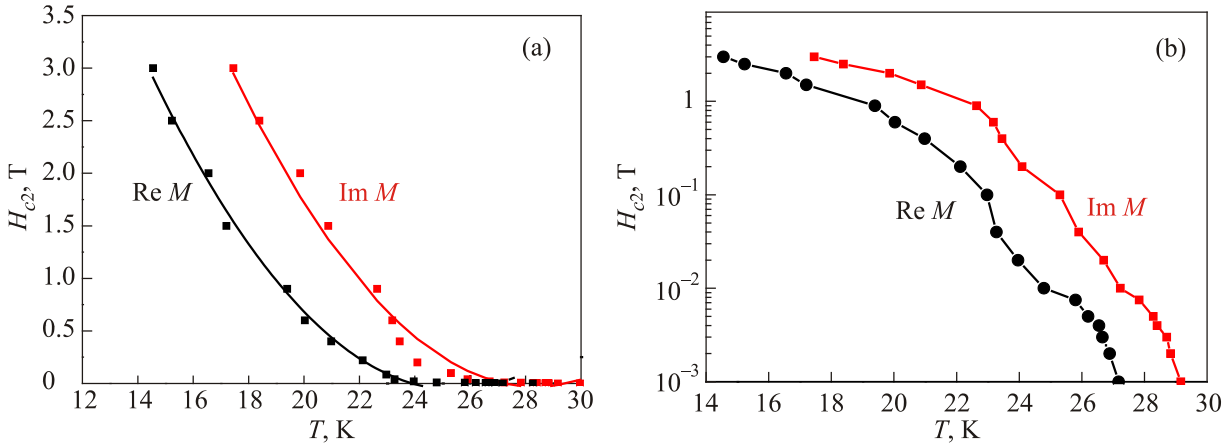

Fig. 6. (Color online) (a) $H_{c2}(T)$ determined as the onsets of Re $M(T)$ and Im $M(T)$ field dependences for 1 UC YBCO film. (b) The same data, on the log scale. The solid lines are guides to the eye.

Acknowledgments

We are grateful to V.F. Gantmakher and R. Huguenin for helpful discussions. We would like to thank S. Zlobin for experimental aid. This work was supported in part by the Russian Academy of Sciences Program "Quantum mesoscopic and nonhomogeneous systems" and RFFI grant 12-02-00171. The work at Brookhaven National Laboratory was supported by the U.S. Department of Energy, Basic Energy Sciences, Materials Sciences and Engineering Division.

1. J.M. Kosterlitz and D.J. Thouless, *J. Phys. C* **6**, 1181 (1973); *Prog. Low Temp. Phys. B* **7**, 373 (1978).
2. M. Rasolt, T. Edis, and Z. Tesanovic, *Phys. Rev. Lett.* **66**, 2927 (1991).
3. P. Minnhagen and P. Olsson, *Phys. Rev. B* **45**, 5722 (1992).
4. T. Terashima, K. Shimura, Y. Bando, Y. Matsuda, A. Fujiyama, and S. Komiyama., *Phys. Rev. Lett.* **67**, 1362 (1991).
5. C. Kwon, Qi Li, X.X. Xi, S. Bhattacharya, C. Doughty, T. Venkatesan, H. Zhang, J.W. Lynn, J.L. Peng, Z.Y. Li, N.D. Spencer, and K. Feldman, *Appl. Phys. Lett.* **62**, 1289 (1993).
6. M.Z. Cieplak, S. Guha, S. Vadlamannati, T. Giebultowicz, and P. Lindenfeld, *Phys. Rev. B* **50**, 12876 (1994).
7. V.A. Gasparov, G.E. Tsydynzhapov, I.E. Batov, and Qi Li, *J. Low Temp. Phys.* **139**, 49 (2005).
8. J.M. Repaci, C. Kwon, Qi Li, X. Jiang, T. Venkatessan, R.E. Glover, III, C.J. Lobb, and R.S. Newrock, *Phys. Rev. B* **54**, 9674 (1996).
9. M.C. Sullivan, T. Frederiksen, J.M. Repaci, D.R. Strachan, R.A. Ott, and C.J. Lobb, *Phys. Rev. B* **70**, 140503(R) (2004).
10. A. Gurevich and V.M. Vinokur, *Phys. Rev. Lett.* **100**, 227007 (2008).
11. M.R. Beasley, J.E. Mooij, and T.P. Orlando, *Phys. Rev. Lett.* **42**, 1165 (1979).
12. A.T. Fiory, A.F. Hebard, P.M. Mankiewich, and R.E. Howard, *Phys. Rev. Lett.* **61**, 19 (1988).
13. L.C. Davis, M.R. Beasley, and D.J. Scalapino, *Phys. Rev. B* **42**, 99 (1990).
14. C.T. Rogers, K.E. Myers, J.N. Eckstein, and I. Božović, *Phys. Rev. Lett.* **69**, 160 (1992).
15. P. Minnhagen, *Rev. Mod. Phys.* **59**, 1001 (1987).
16. V. Ambegaokar, B.I. Halperin, D.R. Nelson, and E.D. Siggia, *Phys. Rev. Lett.* **40**, 783 (1978); *Phys. Rev. B* **21**, 1806 (1980).
17. B.J. Halperin and D.R. Nelson, *J. Low Temp. Phys.* **36**, 599 (1979).
18. J. Bardeen and M.J. Stephen, *Phys. Rev.* **140**, A1197 (1965).
19. V. Gasparov, E. Zhukova, A. Voronkov, B. Gorshunov, and Qi Li, *J. Phys.: Conf. Ser.* **150**, 052058 (2009).
20. V.A. Gasparov and I. Božović, *Phys. Rev. B* **86**, 094523 (2012).
21. V.A. Gasparov, Xi He, G. Dubuis, D. Pavuna, N.D. Kusch, E.B. Yagubskii, J.A. Schlueter, and I. Božović, *Int. J. Mod. Phys. B* **29**, 1542012 (2015).
22. I. Božović, *IEEE Trans. Appl. Supercond.* **11**, 2686 (2001).
23. A. Gozar, G. Logvenov, L. Fitting Kourkoutis, A.T. Bollinger, L.A. Giannuzzi, D.A. Muller, and I. Božović, *Nature* **455**, 782 (2008).
24. G. Logvenov, A. Gozar, and I. Božović, *Science* **326**, 699 (2009).
25. V.A. Gasparov and A.P. Oganesyan, *Physica C* **178**, 445 (1991).
26. A. Gauzzi, J. Le Cochec, G. Lamura, B.J. Jönsson, V.A. Gasparov, F.R. Ladan, Placais, P.A. Probst, D. Pavuna, and J. Bok, *Rev. Sci. Instrum.* **71**, 2147 (2000).
27. A.T. Fiory, A.F. Hebard, P.M. Mankiewich, and R.E. Howard, *Appl. Phys. Lett.* **52**, 2165 (1988).
28. J.L. Jeanneret, G.A. Gavilano, A. Racine, C. Leemann, and P. Martinoli, *Appl. Phys. Lett.* **55**, 2336 (1989).
29. J.H. Claassen, *Appl. Phys. Lett.* **82**, 601 (2003).
30. S.J. Turneaure, A.A. Pesetski, and T.R. Lemberger, *J. Appl. Phys.* **83**, 4334 (1998).
31. V. Gasparov, I. Sheikin, and S. Otani, *Physica C* **178**, 449 (1991).
32. V.A. Gasparov, N.S. Sidorov, and I.I. Zver'kova, *Phys. Rev. B* **73**, 094510 (2006).
33. G. Dubuis, Xi He, and I. Božović, *Rev. Sci. Instrum.* **85**, 103902 (2014).
34. M. Tinkham, *Introduction to Superconductivity*, McGraw Hill, New York (1996), 2nd ed., p. 381.